FEBS Letters

FEBS PRESS science publishing by scientists

Crystal structure of the catalytic domain of the *Weissella oryzae* botulinum-like toxin

Sara Košenina[1], Geoffrey Masuyer[1], Sicai Zhang[2,3,4], Min Dong[2,3,4] and Pål Stenmark[1,5]

1 Department of Biochemistry and Biophysics, Stockholm University, Sweden
2 Department of Urology, Boston Children's Hospital, Boston, MA, USA
3 Department of Microbiology and Immunobiology, Harvard Medical School, Boston, MA, USA
4 Department of Surgery, Harvard Medical School, Boston, MA, USA
5 Department of Experimental Medical Science, Lund University, Sweden

Correspondence
M. Dong, Department of Urology, Boston Children's Hospital, Boston, MA 02115, USA
Tel: +1 857 218 4232
E-mail: min.dong@childrens.harvard.edu
or
P. Stenmark, Department of Biochemistry and Biophysics, Stockholm University, SE-106 91 Stockholm, Sweden
Tel: +46 8 16 37 29
E-mail: stenmark@dbb.su.se

(Received 30 April 2019, revised 15 May 2019, accepted 16 May 2019, available online 31 May 2019)

doi:10.1002/1873-3468.13446

Edited by Maurice Montal

Botulinum neurotoxins (BoNTs) are the most potent toxins known. So far, eight serotypes have been identified that all act as zinc-dependent endopeptidases targeting SNARE proteins and inhibiting the release of neurotransmitters. Recently, the first botulinum toxin-like protein was identified outside the Clostridial genus, designated BoNT/Wo in the genome of *Weissella oryzae*. Here, we report the 1.6 Å X-ray crystal structure of the light chain of BoNT/Wo (LC/Wo). LC/Wo presents the core fold common to BoNTs but has an unusually wide, open and negatively charged catalytic pocket, with an additional Ca^{2+} ion besides the zinc ion and a unique ß-hairpin motif. The structural information will help establish the substrate profile of BoNT/Wo and help our understanding of how BoNT evolved.

Keywords: botulinum neurotoxin; *Weissella oryzae*; X-ray crystallography; zinc endopeptidase

Botulinum neurotoxins (BoNTs) are the most toxic proteins known. They are produced by the spore-forming bacteria *Clostridium botulinum* and are the causative agents of botulism [1]. Despite the threat posed by BoNTs, their cellular and substrate specificity allows utilising the toxins for treatment of human diseases related to hyperactive nerve terminals, such as movement disorders and pain syndromes [2,3]. To this date, eight distinct serotypes of BoNTs have been identified and characterised (BoNT/A-G, /X) [1,2,4]. So far, BoNTs have been reported to target only mammals, fish and birds [5], although their substrates, SNARE proteins, are widespread across eukaryotes [6].

Clostridium neurotoxins (CNTs) have a distinct architecture consisting of three domains. Each domain has a unique function – the heavy chain (HC) (~100 kDa) encompasses a translocation (H_N) and a receptor-binding domain (H_C) while the light chain (LC) (~50 kDa) exhibits the catalytic function [1].

Upon their entry into the circulatory system, BoNTs specifically target presynaptic motoneurons by recognition and binding to ganglioside and protein receptors, followed by receptor-mediated endocytosis. The acidic pH in the endosome causes conformational changes, leading to insertion of HC into the endosomal membrane, and translocation of LC into the cytosol. Once the active LC reaches the cytosol it acts as an endoprotease, cleaving one of the members of the SNARE (soluble N-ethylmaleimide-sensitive factor attachment protein receptor) protein family. BoNT/A, /C and /E cleave the peripheral membrane protein SNAP-25. BoNT/B, /D, /F, /G and /X cleave the vesicle-associated membrane

Abbreviations
BoNT, botulinum neurotoxin; CNTs, clostridium neurotoxins; HC, heavy chain; LC, light chain; Wo, *Weissella oryzae*.

protein VAMP1/2/3. BoNT/C can also cleave syntaxin 1 [7]. In addition, BoNT/X can cleave VAMP4/5 and Ykt6. The cleavage blocks neurotransmitter release and causes flaccid paralysis and when left untreated lethal repression of the respiratory system [8,9].

Bioinformatic analysis of the genome of *Weissella oryzae* (*W. oryzae*) strain SG25 recently revealed the first CNT homologue outside the clostridial genome, designated BoNT/Wo [10,11]. *W. oryzae* is a gram-positive, nonspore-forming anaerobic bacteria isolated from fermented rice grains and is distantly related to *C. botulinum* [12]. Despite a very low overall sequence identity with other BoNTs, the typical CNT tri-domain architecture is conserved in BoNT/Wo, with the highest homology observed for the catalytic domain (average 18.7% sequence identity with other LCs) [10]. LC/Wo has been shown to cleave rat VAMP2 *in vitro* at a unique cleavage site within a juxtamembrane segment (Trp89-Trp90), although whether VAMP2 in neurons can be cleaved by BoNT/Wo remains to be examined [11]. The natural BoNT/Wo targets have not been established.

All BoNT LCs crystal structures have been resolved [13–21] and show a highly conserved globular fold, with mixed secondary structures of α-helices and β-strands. The catalytic pocket, including the conserved HExxE zinc-dependent protease motif, has similar composition and geometries across all LCs. Slight variations in the structure and surface properties are likely to determine substrate and cleavage site specificity.

In order to characterise and identify the function of BoNT/Wo, we solved the X-ray crystal structure of its catalytic domain, LC/Wo, at high resolution (1.6Å). We show that LC/Wo exhibits a fold similar to that of other BoNTs, but also presents unique features that suggest a distinct substrate binding mechanism.

Materials and methods

Cloning, expression and purification of LC/Wo

LC/Wo was sub-cloned into pET28a vector via restriction enzyme site, NdeI and BamHI with a His-tag fused to the N terminus. The gene for native LC/Wo was expressed in *E. coli* BL21 (DE3) T1R pRARE2 in TB medium in the presence of kanamycin and chloramphenicol. Cultures were grown at 37 °C until reaching an OD_{600} of 2 when the temperature was reduced to 18 °C. Protein expression was induced at an OD_{600} of 3 with 0.5 mM IPTG. The protein was purified using Ni-NTA affinity chromatography followed by size exclusion chromatography. The His-tag was removed by thrombin cleavage. Sample purity was assessed by SDS/PAGE.

SeMet LC/Wo was produced as per native with exception of the media, cells were grown in M9. Amino acid mix was added when inducing at an OD_{600} of 1.5.

LC/Wo crystallisation and structure determination

Crystals of native LC/Wo were grown overnight at 21 °C using the sitting drop vapour-diffusion method in 96-well sitting drop plates (Swissci). Crystals were obtained mixing 150 nL of protein at 10 mg·mL^{-1} with 50 nL of reservoir solution containing 0.1 M MES pH 6.0, 0.2 M $CaCl_2$ and 20% w/v PEG 6000.

Crystals of SeMet-LC/Wo grew within a week at 21 °C, using the hanging drop vapour-diffusion method. Initial crystal screening was performed in 96-well sitting drop plates (Swissci), optimisation of the crystallisation conditions was performed using 24-well Linbro plates, using streak seeding. Final crystals were obtained by mixing 1 μL of protein at 10 mg·mL^{-1} with 1 μL of reservoir solution containing 0.1 M MES pH 6.0, 0.2 M $CaCl_2$ and 20% w/v PEG 6000. The crystals were cryoprotected (reservoir solution supplemented with 10% v/v glycerol) and flash-frozen in liquid nitrogen for data collection.

A complete dataset to a resolution of 1.6 Å was collected at 100 K, at the I03 station of the Diamond Light Source (UK). Raw data images were processed with XDS [22] and AIMLESS [23] using the CCP4 SUITE 7.0 [24]. The structure was solved using experimental phasing (SAD) (Table 1). The working model was refined using REFMAC5 [25] and phenix.refine [26]. Manual adjustments were done using COOT [27]. Water was added using AutoBuild (Phenix) [28]. Validation was performed with MOLPROBITY [29]. Crystallographic data statistics are summarised in Table 1. All figures were drawn with PyMOL (Schrödinger, LLC, New York).

Results and Discussion

Crystal structure of LC/Wo

LC/Wo (residues 1–475) was recombinantly produced in *E. coli* with a cleavable N-terminal polyhistidine tag. Although crystals of the native protein were obtained, the structure could not be determined by molecular replacement with the existing LC models, likely because of the low sequence identity (~20%) and significant structural differences compared to BoNT/A-G, BoNT/X and the tetanus neurotoxin. LC/Wo was therefore produced with selenomethionine and crystallised in similar conditions. The X-ray structure was determined by experimental phasing using single-wavelength anomalous diffraction (SAD). After optimisation, the crystals diffracted to high resolution and the anomalous signal from the nine SeMet residues

Table 1. Crystallographic statistics of the LC/Wo X-ray structure.

PDB code	6RIM
Space group	P1
No. of molecules in AU	8
Cell dimensions	
a, b, c (Å)	57.9, 105.2, 179.6
α, β, γ (°)	101.7, 90.0, 90.0
Synchrotron source, λ (Å)	Diamond light source (I03), 0.97
Resolution range (Å)	58.63–1.60 (1.63–1.60)
Total reflections	1 895 613
Unique reflections	531 729
Multiplicity	3.6 (3.0)
Completeness (%)	97.1 (89.4)
R_{merge}	0.091 (1.37)
R_{pim}	0.057 (0.96)
I/σ(I)	6.4 (0.99)
$CC_{1/2}$	0.99 (0.37)
Mean B value	29.0
Refinement	
Resolution (Å)	58.63–1.60
R_{cryst} (%)	14.6
R_{free} (%)	19.8
No. of nonhydrogen atoms	
Protein	28 810
Ion	16
Water	3602
R.m.s. deviations	
Bond lengths (Å)	0.006
Bond angles (°)	1.34
Ramachandran plot (%)	
Favoured	96.38
Outliers	0.9

Values in parentheses correspond to the high resolution shell.

allowed for structure determination at a resolution of 1.6 Å (Table 1). Analysis of the data showed pseudo-translational symmetry, and the structure was solved in the space group P1 with eight molecules per asymmetric unit. LC/Wo behaves as a monomer in solution (Fig. S1). The symmetry is a result of crystallisation with the eight monomers presenting nearly identical structures [root mean square deviation (rmsd) values from 0.3 to 0.6 Å].

The electron density is well defined for all residues, with the exception of the C-terminal (residues 458–477), which reaches into the solvent accessible area and is likely to be disordered, as well as loops 232–235 and 280–290 that are disordered in all chains except E and H.

The structure of LC/Wo presents a globular fold similar to other BoNTs and has largely conserved secondary structure elements despite the low sequence homology (20%, Fig. 1). The structure of LC/Wo was compared to the other BoNT LCs using DALI [30] and presented a high degree of similarity reflected by Z-scores ≥ 29, and low rmsd values, which vary between 2.8 and 3.3 Å. Alignment of the 3D structure against all deposited protein data bank (PDB) entries revealed that LC/Wo has the highest structural similarity to LC/X even though it exhibits the lowest sequence identity amongst the light chains (Table 2, Fig. 1B).

One of the most striking structural differences between LC/Wo and other BoNT LCs is the central region of residues 31–60, which presents a twisted β-hairpin. In other LCs, this region forms two short β-strands (between 4 and 7 aa long), connected by an approximately 16-residue long flexible loop facing the solvent accessible area. In LC/Wo this region is formed by a noticeably longer (14 aa), rigid and twisted β-hairpin (Fig. 1A).

Another remarkable difference is the α-helix formed by residues 309–350. While the corresponding helix in other LCs is continuous, in LC/Wo it is interrupted by an extended loop (res 325–338), rich in surface-exposed negatively charged residues, and contains a β-turn (Fig. 1A).

Metal coordination site

LC/Wo contains the conserved, tetrahedral His-Glu-X-X-His + Glu zinc-binding motif, typical for the M27 metallo-peptidases family [31]. The catalytic zinc ion is coordinated by His250, Glu296 and His254, with the fourth coordination completed by a water-mediated bond to Glu251. LC/Wo is likely to follow a similar catalytic mechanism to other BoNTs [7], by deprotonating a water molecule to produce a nucleophile base necessary for the proteolytic activity. In addition, the conserved Arg409 and Tyr412, which are believed to stabilise catalytic intermediates and necessary for activity [32], are within close distance of the active site, congruent with its presumed function (Fig. 2).

A calcium ion was observed in all LC/Wo monomers, ~8 Å from the active site. It presented a classical octahedral geometry, coordinated by six water molecules and Glu198 (Fig. 2; Fig. S2). Proximity of the calcium ion to the active site suggests it might be important for substrate binding. LC/Wo consistently crystallised in the presence of calcium chloride. Any potential role for Ca^{2+} should be investigated further, as it cannot be excluded that the presence of this ion only results from crystallisation.

Access to the active site

Entrance to the catalytic pocket is flanked on one side by the tip of the β-hairpin described above (residues 45–50), and on the other side by loops 205–211 and 261–292 (Fig. 3). The S sub-pocket does not seem to be conserved in comparison to other BoNTs – it

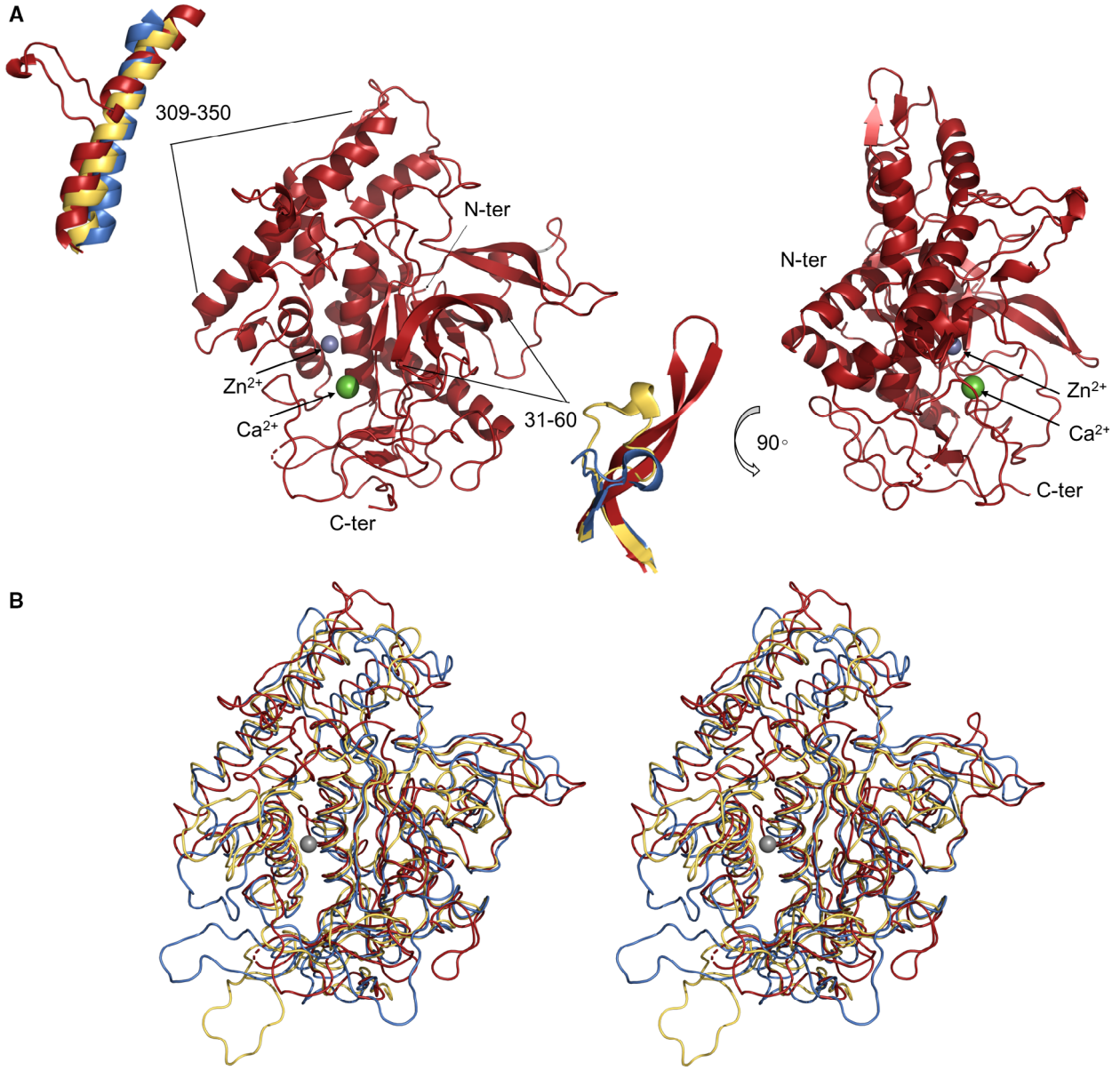

Fig. 1. Crystal structure of LC/Wo and it's unique features in comparison to structures of other BoNT LCs. (A) Ribbon representation of LC/Wo, the zinc ion (grey sphere), calcium ion (green sphere) and other regions of interest are highlighted. Unique features of LC/Wo (red) were superposed with the corresponding regions in LC/X (yellow, PDB 6F47) and LC/B (blue, PDB 1F82). (B) Comparison of LC/Wo with other VAMP-cleaving toxins in 3D stereo representation. LCs of serotypes X and B were superposed with LC/Wo.

consists of a 14 residue long, flexible loop (res 258–272), that likely provide the binding pocket with the plasticity to accommodate the substrate. The S′ subpocket with loops 227–232 and 409–414 is well conserved (Fig. 3A) and includes Arg409 and Tyr412, which are likely also important for substrate recognition, in addition to their role in catalysis [32].

LC/X, the closest structural homolog of LC/Wo, presented restricted access to its active site [21]. LC/Wo on the contrary seems to have an open, negatively charged active site, a property shared with LC/B, which consistently has the highest sequence identity (~22%) to LC/Wo (Fig. 3B) and could share the same substrates [10,11]. Additionally, the catalytic pocket of LC/Wo is wider than any other BoNT catalytic pocket, with an ~25 Å-wide cleft. The negative surface potential is particularly more pronounced in LC/Wo compared to other BoNT LCs (Fig. 3B).

Table 2. Pairwise comparison of LC/Wo with other clostridial neurotoxins using Dali [30] and Needle (EMBOSS server).

		Dali					Needle		
	PDB	rmsd (Å)	No. of aligned positions	No. of residues in matched structure	Sequence identity of aligned positions (%)	*Z* score	Sequence similarity (%)	Sequence identity (%)	Score
LC/X	6F47	2.8	359	427	20	28.7	28	17	128
LC/F	2A97	2.9	366	424	18	30.0	34	19	146
LC/E	1T3a	3.0	362	429	21	29.4	33	20	138
LC/B	1F82	3.0	358	414	19	29.8	36	22	158
LC/D	2Fpq	3.2	355	400	19	31.4	36	22	176
LC/C	2QN0	3.2	348	392	21	30.9	36	21	162
LC/G	1ZB7	3.2	352	414	19	29.4	35	21	162
LC/A	1XTF	3.2	356	413	20	31.3	37	21	208
LC/Te	1Z7H	3.3	362	426	18	30.0	38	21	144

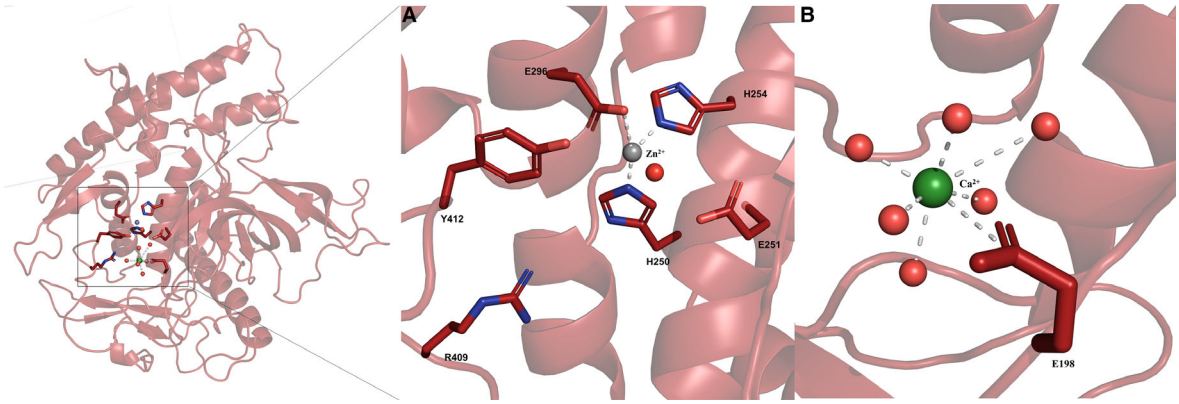

Fig. 2. Metal ion coordination. (A) Zinc ion coordination. (B) Calcium ion coordination. Residues involved in proteolysis are represented as sticks, zinc ion, calcium ion and water molecule as grey, green and red spheres respectively.

Comparison to LC/F-VAMP structure

The structure of LC/Wo presents a groove that extends from the catalytic site and goes around the enzyme (Fig. 3A) in a feature that is conserved across all BoNTs. In particular, this groove was shown to interact with the belt region of the HC in other holotoxins [7] (Fig. S3), and to be involved in substrate binding. The structure of LC/A bound to SNAP25 [33] first illustrated the complex mechanism of the toxin-substrate interaction which consists of multiple exosites. The structure of LC/F in complex with a VAMP-derived peptide inhibitor (PDB 3FIE) [34] confirmed the general mechanism and demonstrated that substrate specificity was defined by the exosites.

Comparison of LC/Wo with the structure of LC/F-VAMP inhibitor shows that the unique twisted β-hairpin feature (res 31–60) in LC/Wo comes into close proximity (≤4Å) to the peptide, which suggests a potential involvement in substrate binding (Fig. 4). The comparison also revealed a significant difference at the loop defining exosites 1 and 2 in LC/F (residues 172–182). In LC/Wo, these sites correspond to a much shorter linker (206–211), similar to the one observed in LC/X [21]. Interestingly, the Ca^{2+} ion observed in LC/Wo is situated within bonding distance (~ 3.5 Å) of the superposed VAMP peptide (Fig. 4), on the opposite side of Zn^{2+}, and might contribute to substrate binding.

Furthermore, comparison of the superposed structures indicated that the substrate's P1 site is likely to interact with Phe258, Asn264, Glu295 and the P1' site with Glu198, Thr247, Arg409 and Tyr412 of LC/Wo (Fig. 3A). The large catalytic pocket, and predicted adaptability of the surrounding loops, would indicate that this site may accommodate the bulky side chains of the suggested cleavage site, W89–W90 of VAMP2 [11]. However, the properties exhibited by the open catalytic pocket, in particular its strong electrostatic potential, suggest that BoNT/Wo may have other substrates.

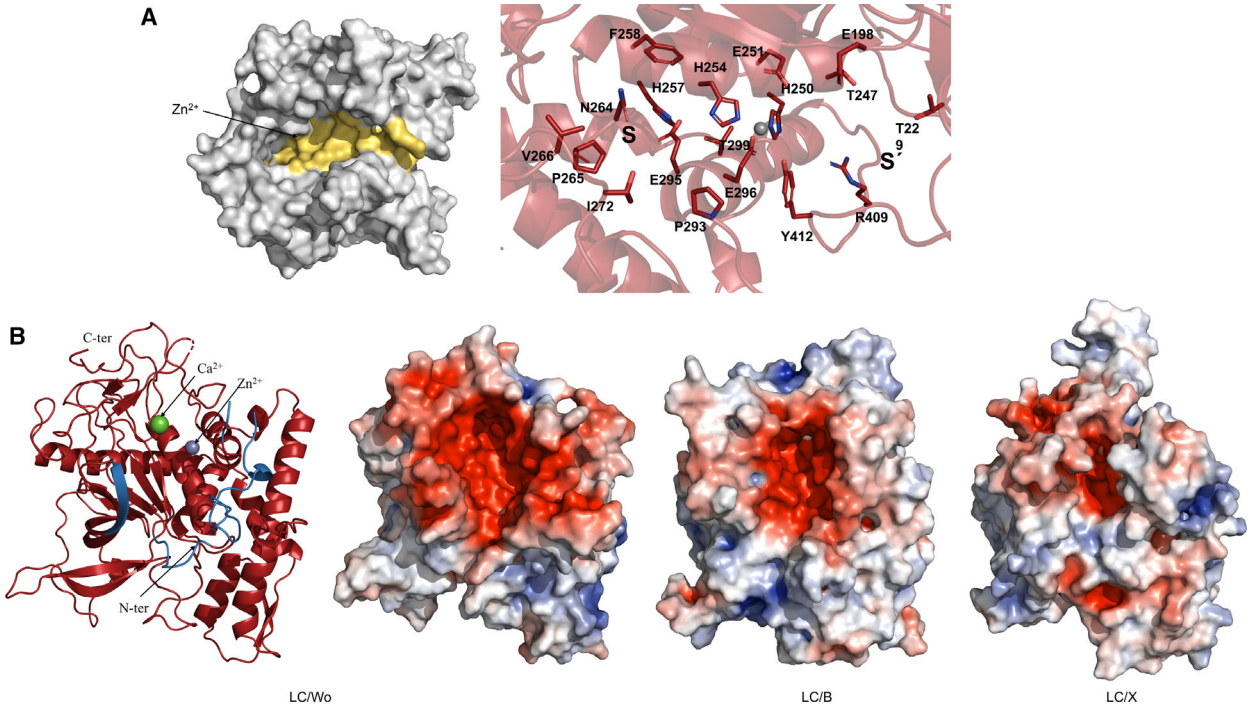

Fig. 3. Catalytic cleft and surface potential of LC/Wo. (A) Left, residues forming the catalytic cleft and potential exosites highlighted in yellow, the surface of LC/Wo is shown in grey; right, close-up view of LC/Wo catalytic pocket and potential substrate binding sites. (B) Left, ribbon representation of LC/Wo with regions flanking the catalytic pocket highlighted in blue; right, surface representation of LC/Wo, /B and /X with electrostatic potential calculated using PyMol's APBS.

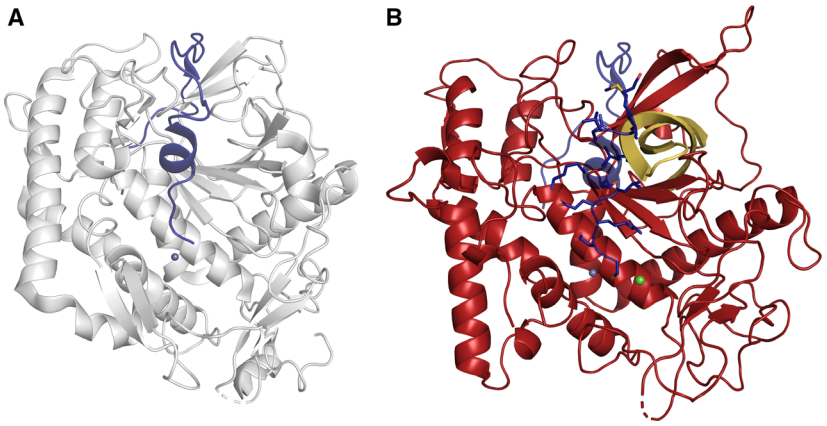

Fig. 4. Potential binding of VAMP in LC/Wo, based on comparison of LC/Wo to LC/F in complex with VAMP-derived peptide inhibitor (PDB 3FIE). (A) LC/F in complex with VAMP-derived peptide inhibitor. LC/F is shown in grey and VAMP-derived inhibitor is shown in blue. (B) LC/Wo was superposed with the structure of LC/F in complex with VAMP-derived peptide inhibitor (PDB 3FIE). LC/Wo is shown in red and VAMP-derived inhibitor is shown in blue sticks (LC/F is not shown). Zinc is shown as grey sphere and calcium is shown as green sphere. Twisted β-hairpin is highlighted in yellow.

Conclusions

In summary, the structure of LC/Wo shows that BoNT/Wo indeed belongs to a superfamily of BoNT zinc-proteases through a common fold. The structure highlighted several unique features, such as a wide and open active site. It also revealed a calcium ion and secondary structure elements involved in the catalytic pocket architecture, which allowed us to suggest potential substrate

binding sites. The structure hints at LC/Wo being a promiscuous enzyme, future work is required to identify potential substrates beyond VAMP2, and alternative target species, including insects.

Acknowledgements

We thank the scientists at stations I03 of the Diamond Light Source (UK, allocation MX15806) for their support during X-ray data collection. We also thank PSF for protein production. This study was supported by the Swedish Research Council (2018-03406) and the Swedish Cancer Society (to PS), by National Institute of Health (NIH) grants (R01NS080833, R01AI132387, R01AI139087, and R21NS106159 to M.D.). M.D. holds the Investigator in the Pathogenesis of Infectious Disease award from the Burroughs Welcome Fund.

Author contributions

PS and MD conceived the project and supervised the study. SK, GM and PS designed experiments; SK and SZ performed experiments; SK and GM analysed data; SK wrote the manuscript; GM, PS and MD made manuscript revisions.

Data availability

The atomic coordinates and structure factors (code 6RIM) have been deposited in the Protein Data Bank (http://wwpdb.org).

References

1 Montal M (2010) Botulinum neurotoxin: a marvel of protein design. *Ann Rev Biochem* **79**, 591–617.
2 Montecucco C and Molgo J (2005) Botulinal neurotoxins: revival of an old killer. *Curr Opin Pharmacol* **5**, 274–279.
3 Angaut-Petit D, Juzans P, Molgo J, Faille L, Seagar MJ, Takahashi M and Shoji-Kasai Y (1995) Mouse motor nerve terminal immunoreactivity to synaptotagmin II during sustained quantal transmitter release. *Brain Res* **681**, 213–217.
4 Zhang S, Masuyer G, Zhang J, Shen Y, Lundin D, Henriksson L, Miyashita SI, Martinez-Carranza M, Dong M and Stenmark P (2017) Identification and characterization of a novel botulinum neurotoxin. *Nat Commun* **8**, 14130.
5 Smith LDS and Sugiyama H (1988) Botulism. The organism, its toxins, the disease. Charles C Thomas, Springfield, IL.
6 Ungar D and Hughson FM (2003) SNARE protein structure and function. *Annu Rev Cell Dev Biol* **19**, 493–517.
7 Rossetto O, Pirazzini M and Montecucco C (2014) Botulinum neurotoxins: genetic, structural and mechanistic insights. *Nat Rev Microbiol* **12**, 535–549.
8 Swaminathan S (2011) Molecular structures and functional relationships in clostridial neurotoxins. *FEBS J* **278**, 4467–4485.
9 Dong M, Masuyer G and Stenmark P (2018) Botulinum and Tetanus Neurotoxins. *Ann Rev Biochem* **88**, 2.1–2.27.
10 Mansfield MJ, Adams JB and Doxey AC (2015) Botulinum neurotoxin homologs in non-Clostridium species. *FEBS Lett* **589**, 342–348.
11 Zornetta I, Azarnia Tehran D, Arrigoni G, Anniballi F, Bano L, Leka O, Zanotti G, Binz T and Montecucco C (2016) The first non *Clostridial botulinum*-like toxin cleaves VAMP within the juxtamembrane domain. *Sci Rep* **6**, 30257.
12 Tohno M, Kitahara M, Inoue H, Uegaki R, Irisawa T, Ohkuma M and Tajima K (2013) Weissella oryzae sp. nov., isolated from fermented rice grains. *Int J Syst Evol Microbiol* **63**, 1417–1420.
13 Swaminathan S and Eswaramoorthy S (2000) Structural analysis of the catalytic and binding sites of *Clostridium botulinum* neurotoxin B. *Nat Struct Biol* **7**, 693–699.
14 Agarwal R, Eswaramoorthy S, Kumaran D, Binz T and Swaminathan S (2004) Structural analysis of botulinum neurotoxin type E catalytic domain and its mutant Glu212fGln reveals the pivotal role of the Glu212 carboxylate in the catalytic pathway. *Biochemistry* **43**, 6637–6644.
15 Segelke B, Knapp M, Kadkhodayan S, Balhorn R and Rupp B (2004) Crystal structure of *Clostridium botulinum* neurotoxin protease in a product-bound state: evidence for noncanonical zinc protease activity. *Proc Natl Acad Sci USA* **101**, 6888–6893.
16 Agarwal R, Binz T and Swaminathan S (2005) Structural analysis of Botulinum neurotoxin serotype F Light Chain: implications on substrate binding and inhibitor design. *Biochemistry* **44**, 11758–11765.
17 Arndt JW, Yu W, Bi F and Stevens RC (2005) Crystal structure of botulinum neurotoxin type G light chain: serotype divergence in substrate recognition. *Biochemistry* **44**, 9574–9580.
18 Breidenbach MA and Brunger AT (2005) 2.3 Å crystal structure of tetanus neurotoxin light chain. *Biochemistry* **44**, 7450–7457.
19 Arndt JW, Christian QCT and Stevens RC (2006) Structure of Botulinum neurotoxin type D light chain at 1.65 Å resolution: repercussions for VAMP-2 substrate specificity. *Biochemistry* **45**, 3255–3262.
20 Jin R, Sikorra S, Stegmann CM, Pich A, Binz T and Brunger AT (2007) Structural and biochemical studies of Botulinum neurotoxin serotype C1 light chain protease: implications for dual substrate specificity. *Biochemistry* **46**, 10685–10693.

21 Masuyer G, Zhang S, Barkho S, Shen Y, Henriksson L, Kosenina S, Dong M and Stenmark P (2018) Structural characterisation of the catalytic domain of botulinum neurotoxin X - high activity and unique substrate specificity. *Sci Rep* **8**, 4518.
22 Kabsch W (2010) Xds. *Acta Crystallogr D Biol Crystallogr* **66**, 125–132.
23 Evans P (2006) Scaling and assessment of data quality. *Acta Crystallogr D Biol Crystallogr* **62**, 72–82.
24 Collaborative Computational Project N (1994) The CCP4 suite: programs for protein crystallography. *Acta Cryst* **D50**, 760–763.
25 Murshudov GN, Skubak P, Lebedev AA, Pannu NS, Steiner RA, Nicholls RA, Winn MD, Long F and Vagin AA (2011) REFMAC5 for the refinement of macromolecular crystal structures. *Acta Crystallogr D Biol Crystallogr* **67**, 355–367.
26 Afonine PV, Grosse-Kunstleve RW, Echols N, Headd JJ, Moriarty NW, Mustyakimov M, Terwilliger TC, Urzhumtsev A, Zwart PH and Adams PD (2012) Towards automated crystallographic structure refinement with phenix.refine. *Acta Crystallogr D Biol Crystallogr* **68**, 352–367.
27 Emsley P, Lohkamp B, Scott WG and Cowtan K (2010) Features and development of Coot. *Acta Crystallogr D Biol Crystallogr* **66**, 486–501.
28 Terwilliger TC, Grosse-Kunstleve RW, Afonine PV, Moriarty NW, Zwart PH, Hung LW, Read RJ and Adams PD (2008) Iterative model building, structure refinement and density modification with the PHENIX AutoBuild wizard. *Acta Crystallogr D Biol Crystallogr* **64**, 61–69.
29 Chen VB, Arendall WB 3rd, Headd JJ, Keedy DA, Immormino RM, Kapral GJ, Murray LW, Richardson JS and Richardson DC (2010) MolProbity: all-atom structure validation for macromolecular crystallography. *Acta Crystallogr D Biol Crystallogr* **66**, 12–21.
30 Hasegawa H and Holm L (2009) Advances and pitfalls of protein structural alignment. *Curr Opin Struct Biol* **19**, 341–348.
31 Rawlings ND, Barrett AJ, Thomas PD, Huang X, Bateman A and Finn RD (2018) The MEROPS database of proteolytic enzymes, their substrates and inhibitors in 2017 and a comparison with peptidases in the PANTHER database. *Nucleic Acids Res* **46**, D624–D632.
32 Binz T, Bade S, Rummel A, Kollewe A and Alves J (2001) Arg362 and Tyr365 of the botulinum neurotoxin type A light chain are involved in transition state stabilization. *Biochemistry* **41**, 1717–1723.
33 Brunger MABAT (2004) Substrate recognition strategy for botulinum neurotoxin serotype A. *Letters Nat* **432**, 925–929.
34 Agarwal R, Schmidt JJ, Stafford RG and Swaminathan S (2009) Mode of VAMP substrate recognition and inhibition of *Clostridium botulinum* neurotoxin F. *Nat Struct Mol Biol* **16**, 789–794.

Supporting information

Additional supporting information may be found online in the Supporting Information section at the end of the article.

Fig. S1. SDS/PAGE gel and trace from gel filtration of LC/Wo.

Fig. S2. Metal coordination site (chain E).

Fig. S3. Superposition of LC/Wo with BoNT/B.